Desalination and Water Treatment
www.deswater.com

doi: 10.5004/dwt.2021.27430

230 (2021) 318–330
August

Enhanced photocatalytic degradation of Congo red under visible light illumination by using Zn-Al-Co-LDH@g-C_3N_4 nanocomposite

Mohamad Ajam[a,*], Majid Ehteshami[a], Siamak Boudaghpour[a], Seyyed Ahmad Mirbagheri[a], Mahbubeh Kafil[b]

[a]*Department of Environmental Engineering, Faculty of Civil Engineering, K.N. Toosi University of Technology, Tehran, Iran, Tel. +989125730693; email: m_ajam88@yahoo.com (M. Ajam), Tel. +989121147833; email: ehteshami@kntu.ac.ir (M. Ehteshami), Tel. +989226308832; email: bodaghpour@kntu.ac.ir (S. Boudaghpour), Tel. +989121374357; email: mirbagheri@kntu.ac.ir (S.A. Mirbagheri)*

[b]*Department of Environmental and Biological Sciences, University of Eastern Finland, P.O. Box: 1627, FI-70211 Kuopio, Finland, Tel. +358 414708731; emails: makafil@uef.fi/m-kafil@phdstu.scu.ac.ir*

Received 2 August 2020; Accepted 10 May 2021

ABSTRACT

In this study, the potential of layered double hydroxide (Zn-Co-Al) decorated with g-C_3N_4 (CN) as a novel nanocomposite for degradation of Congo red (CR) under ultrasonic irradiation was evaluated. Characterization studies including transmission electron microscopy, scanning electron microscopy, X-ray diffraction, Brunauer–Emmett–Teller, Fourier-transform infrared spectroscopy and ultraviolet-visible diffuse reflectance spectroscopy (UV-Visible DRS) were conducted to study the structure of synthesized nanocomposite. Such characteristics as an open hierarchical structure comprised of intertwined CN and Zn-Al-Co-LDH nanosheets make it an efficient photocatalyst for the removal of anionic pollutants from water under simulated sunlight irradiation. The degradation efficiency of Congo red (CR) with Zn-Al-Co-LDH@CN catalyst was 92.7%. Regarding the effect of scavengers on the dye, ethylenediaminetetraacetic acid had a higher value than ethanol and benzoquinone (BQ) implying the considerable role of the hole (h^+) in decomposing CR compared to the insignificant role of $OH^\bullet$ and $O_2^\bullet$. During five sequential runs, a decline of less than 10% was observed in the removal efficiency of CR. The removal efficiency of chemical oxygen demand and total organic carbon was approximately 71% and 52%, respectively, within 400 min confirming the mineralization of CR.

Keywords: Photocatalysis; Anionic dye; Layered double hydroxide; g-C_3N_4; Visible light

1. Introduction

With the rapid rate of the world's population growth and the high speed of industrialization over the last century, water resource contamination has been inevitable [1]. Wastewater effluents generated from industrial activities can adversely affect the biota and fauna. Among the existing industrial branches, the textile industry consumes a vast quantity of water and consequently disposes a significant amount of wastewater. These effluents contain several perilous chemicals such as acids, alkalis, dyes, surfactants and other inorganic and organic contaminants [2]. Congo red (CR) is among common anionic water-soluble dyes applied in cotton textile and cellulose industries and can pose a risk to the aquatic environment even in low concentrations [3]. Different methods such as chemical [4], advanced oxidation process (AOP) [5] biological [6] and physical [7] treatments were previously utilized for removing dye pollutants from

* Corresponding author.

wastewater. Photocatalytic degradation, as one of the AOP processes, offers the most cost-effective approach to the accomplishment of wastewater decontamination.

Photocatalytic degradation of organic pollutants is a green, economic and widely accepted technology; thus, the development of photo-catalyst has been the focus of many studies [8–10]. The layered double hydroxide (LDH) has advantages such as a unique layered structure and tunable composition of the photocatalyst [10]. According to the literature, a series of LDHs is reported to be effective photocatalysts for the treatment of water pollution. Zn– and Co– based LDHs as photocatalysts have superior performance due to their chemical stability and low toxicity [11]. However, pristine monolayer LDH has poor charge mobility and a high density of surface charges. Such characteristics lead to recombination of photogenerated electron-hole pairs and easy aggregation of LDH nanoplates which consequently decrease its photocatalytic activity [12]. Therefore, approaches like metal element doping through co-precipitation are suggested to improve the photocatalytic activity of LDH [13]. Due to its low cost, nontoxicity and having a unique electronic configuration, Co has drawn great attention among other mentioned metal elements [13]. Parida et al. [13] reported that the co-precipitation approach for producing Cu/Cr LDH doped with Co^{2+} demonstrated a super behavior for degradation of malachite green under sunlight illumination. Co-Al-LDH was used as an efficient photocatalyst for oxygen evolution. The efficient photocatalytic performance of Zn-Al-LDH for dye degradation under visible light has been reported [10]. Doping with other metal elements including Tb, Fe, Ce and Ni was also suggested for enhancement of LDH photocatalytic activity [14–17]. In this study, Zn-Al-LDH doped with CO^{2+} showed excellent photocatalytic activity for the degradation of CR.

Although recombination of photogenerated electron–hole pairs may be impeded by metal element doping, the aggregation of LDH nanoplates is still a major challenge. The composite of LDHs and g-C_3N_4 (CN) causes the separation of photogenerated electron-hole pairs in nanocomposites and hinders the aggregation of LDH nanoplates [18]. Some features including appropriate band structure, facile preparation and peculiar physicochemical stability make CN an efficient photocatalyst [19]. LDH nanoplates deposited on CN sheets (LDH/CN) have less aggregation, larger specific surface area, more active sites and consequently more photocatalytic activity [5]. A remarkable improvement in the photocatalytic performance of CN/NiAl-LDH heterostructure compared to CN and LDH for photoconversion of CO_2 to CO under visible-light illumination was reported [20]. Ong et al. [21] developed a hierarchical $ZnIn_2S_4$/CN heterostructure, demonstrating an enhancement in the H_2-generation performance in comparison with the bare $ZnIn_2S_4$ and CN. Similarly, the application of CN-based 2D/2D composites for different photocatalytic applications such as pollutant degradation, H_2 evolution, and CO_2 photoreduction have been reported [22].

The aim of the present study is (a) fabricating and characterizing Zn-Al-Co-LDH@CN composite (b) Optimizing photocatalytic degradation of CR under visible light by modifying operational parameters such as catalyst dosage, pollutant concentration, initial pH of the solution, enhancers and scavengers.

2. Materials and methods

2.1. Chemicals

Chemicals used in this study are $Zn(NO_3)_2{\cdot}6H_2O$, cobalt(II) nitrate hexahydrate ($Co(NO_3)_2{\cdot}6H_2O$), aluminum nitrate nonahydrate $Al(NO_3)_3{\cdot}9H_2O$, urea (CH_4N_2O), hydrogen peroxide (H_2O_2), sodium carbonate (Na_2CO_3), hydrochloric acid (HCl), sodium hydroxide (NaOH), ethanol (CH_3CH_2OH) and p-benzoquinone ($C_6H_4O_2$), potassium peroxydisulfate ($K_2S_2O_8$), ethylenediaminetetraacetic acid (EDTA), sodium chloride (NaCl) and CR ($C_{22}H_{14}N_6Na_2O_9S_2$). All chemicals were purchased from Sigma-Aldrich, Germany.

2.2. Synthesis of Zn-Al-Co-LDH@g-C_3N_4

2.2.1. g-C_3N_4

The bulk g-C_3N_4 (CN) was acquired by polymerizing the melamine molecules at a constant heating rate of 5°C min^{-1} under nitrogen flow and was kept at 600°C for 2 h. Ultrathin CN nanosheets were prepared by mixing 0.5 g as-prepared bulk g-C_3N_4 with 100 mL deionized water using an ultrasonic probe for 15 h. Finally, the suspension was centrifuged at 6,000 rpm for 7 min to harvest CN nanosheets [20].

2.2.2. Zn-Al-Co-LDH

The co-precipitation method was used to synthesize Zn-Al-Co-LDH with a carbonate interlayer. Initially, $Zn(NO_3)_2{\cdot}6H_2O$ (5.94 g), $Co(NO_3)_2{\cdot}6H_2O$ (2.91 g) and $Al(NO_3)_3{\cdot}9H_2O$ (3.75 g) were mixed in 100 mL deionized water (the molar ratio of Zn/Co/Al was approximately (2:1:1) and stirred at room temperature for 30 min. Then, NaOH (2.4 g) and Na_2CO_3 (2.12 g) were blended in 100 mL deionized water to prepare the alkaline solution. The pH value of the metal salt solution was adjusted by the alkaline solution to reach 8.5. Then, the suspension was aged at 333 K for 24 h. At this point, the filtration and washing steps were conducted to remove debris from the final product [23].

2.2.3. Zn-Al-Co-LDH@g-C_3N_4

To obtain a uniform suspension, 0.1 g CN nanosheet was dissolved in 100 mL deionized water for 20 min. After adding metal salt to the CN suspension, the resulting blend was stirred at room temperature (25°C) and ambient atmosphere for 30 min. Then, the alkaline solution was used drop by drop until pH = 8.5 was reached. In the following step, the suspension was aged at 333 K for 24 h. Then, filtration and washing were conducted to remove the excess metal salts. The solid was finally dried and grounded [23].

2.3. Experimental procedure

All experiments for photocatalytic degradation of CR were conducted according to the following procedure.

At the first step, photocatalyst with the optimum dosage was added to 150 mL of CR solution in the range of 30–60 mg L^{-1} concentration. Firstly, to measure the adsorption of the dye contaminant, the photoreactor was stirred in a dark condition for 30 min. Then, the suspension was irradiated with an LED lamp (λ > 420 nm, 300 W, Shenzhen Starvanq Technology, China) for 150 min. Then, 3 mL of samples were withdrawn from the photoreactor at 15 min intervals. The absorbance of residual CR was measured by a UV-Visible spectrophotometer (SU6100 Pillar Scientific, USA) at a maximum wavelength of 497 nm [3]. To examine the mineralization of CR, chemical oxygen demand (COD) analysis was measured by applying Palintest Photometer (United Kingdom) in accordance with the Standard Method No. 5220 [24]. Samples were finally filtrated and dried at 80°C for 8 h for further analysis [5].

2.4. Analysis

The surface area and pore volume were measured by performing transmission electron microscopy (TEM) analysis (Philips, EM208S, 100 kV). To specify the surface morphology and elemental composition of Zn-Al-Co-LDH@CN, a field emission scanning electron microscope (FE-SEM) equipped with an energy-dispersive X-ray spectroscopy (EDX) detector (TESCAN, MIRA-3, Czech Republic) was used. X-ray diffraction analysis (Philips PW 1730, Netherlands) was used to analyze the crystalline structure of Zn-Al-Co-LDH@CN by Cu Kα radiation (λ = 0.154056 nm) at 30 mA and 40 kV. Brunauer–Emmett–Teller (BET) analysis was performed using BELSORP-mini II (Japan) at 77 K. Fourier-transform infrared spectroscopy (FT-IR) analysis (Avatar, Thermo, USA) was used to determine the surface functional groups of Zn-Al-Co-LDH@CN within the range of 400–4,000 cm^{-1} by the KBr disk technique. The bandgap of Zn-Al-Co-LDH and Zn-Al-Co-LDH@CN was determined by UV-Vis spectrophotometer (Japan, Shimadzu). Finally, the Shimadzu TOC 5000A analyzer was applied to measure the total organic carbon by catalytic oxidation method in 680°C combustions.

3. Results and discussion

3.1. Characterization of synthesized nanocomposite

3.1.1. TEM, SEM and EDX results

The formation of nanosheets with regular shapes on the surface of Zn-Al-Co-LDH@CN microspheres and the crystalline morphology of Zn-Al-Co-LDH are observed in TEM images (Fig. 1A).

The results of scanning electron microscopy (SEM) analysis are given in Fig. 1B at various magnifications (200 nm to 1 μm scale). The micromorphology of CN is irregular sheets studied with high resolution (Fig. 1Ba and b). According to Fig. 1Bc and d, the as-synthesized Zn-Al-Co-LDH presents in some microspheres with rather regular shapes. Fig. 1Be and f show that the as-synthesized Zn-Al-Co-LDH@CN consists of microspheres with relatively regular shapes decorated with nanosheets. This nanostructure with exceptional characteristics such as higher specific surface area and further active sites offers high potentials for photocatalytic degradation of CR [24].

EDX analysis was used to study elemental compositions; for CN, peaks for carbon (27.85 wt.%), oxygen (4.15 wt.%) and nitrogen (68.00 wt.%) are observed (Fig. 2a). On the other hand, for Zn-Al-Co-LDH, the sample contains zinc (23.59 wt.%), cobalt (10.96 wt.%), oxygen (55.08 wt.%), aluminum (5.80 wt.%) and nitrogen (4.56 wt.%) (Fig. 2b). However, for Zn-Al-Co-LDH@CN nanocomposite, the EDX result shows peaks that previously was observed in CN and Zn-Al-Co-LDH (Fig. 2c). Results demonstrated the presence of O, N, C, Zn, Co, and Al with weight percent of 50.18%, 4.41%, 6.79%, 23.25%, 10.38% and 4.98%, respectively in the as-synthesized catalyst.

As presented in Fig. 3, the EDX analysis proved that Zn, Co, Al, O, C and N elements were dispersed uniformly all through the nanocomposite surface, implying the formation of a well-organized structure of as-prepared composite as a photocatalyst [11]. Consequently, there is the possibility of strong coupling interaction between two layered materials through electrostatic binding [25].

3.1.2. X-ray diffraction results

The crystalline structures of the CN, Zn-Al-Co-LDH and Zn-Al-Co-LDH@CN were analyzed by X-ray diffraction (XRD). As illustrated in Fig. 4, a strong peak of pure CN is observed in the (002) plane at 27.6°, attributing to the interplanar stacking of the aromatic system. The other weak peak of the (100) plane at 13.1° implies typical interlayer structural packing [26]. For Zn-Al-Co-LDH, all peaks can be well indexed to a typical hexagonal phase (JCPDS no. 51-0045) [27]. Main peaks with 2θ values of 11.5°, 23.2°, 34.4°, 39.0°, 46.5°, 60.0°, and 61.3° are attributed to crystal planes, including (003), (006), (012), (015), (018), (110), and (113), respectively. Although the CN pattern showed an intensive peak at around 27.6°, this peak was not observed in the XRD spectra of Zn-Al-Co-LDH@CN heterojunctions due to the low content of CN and relatively its low diffraction intensity. Similar phenomenon was reported in previous studies regarding the modification of LDHs [21].

3.1.3. BET results

BET analysis was performed for determining the surface area and pore size of pure and synthesized photocatalyst. The N_2 adsorption–desorption isotherms for the Zn-Al-Co-LDH, CN and Zn-Co-Al LDH@CN are shown in Fig. 5. Pores are categorized into three distinct groups: macropores (>50 nm), mesopores (2–50 nm) and micropores (2 nm>) [28]. Regarding IUPAC categorization, the adsorption–desorption isotherms of Zn-Al-Co-LDH, CN and Zn-Al-Co-LDH@CN demonstrate isotherms of type IV with a H_3 hysteresis loop [24]. According to BET results, the specific surface area of Zn-Al-Co-LDH and Zn-Al-Co-LDH@CN are 61.65 and 44.94 $m^2\ g^{-1}$, respectively higher than CN with only 17.74 $m^2\ g^{-1}$. According to Table 1, although the S_{BET} value of Zn-Al-Co-LDH@CN heterojunction is slightly less than Zn-Al-Co-LDH, it clearly showed improved photocatalytic activities. Therefore, it can be inferred that the considerable improvement in the degradation performance

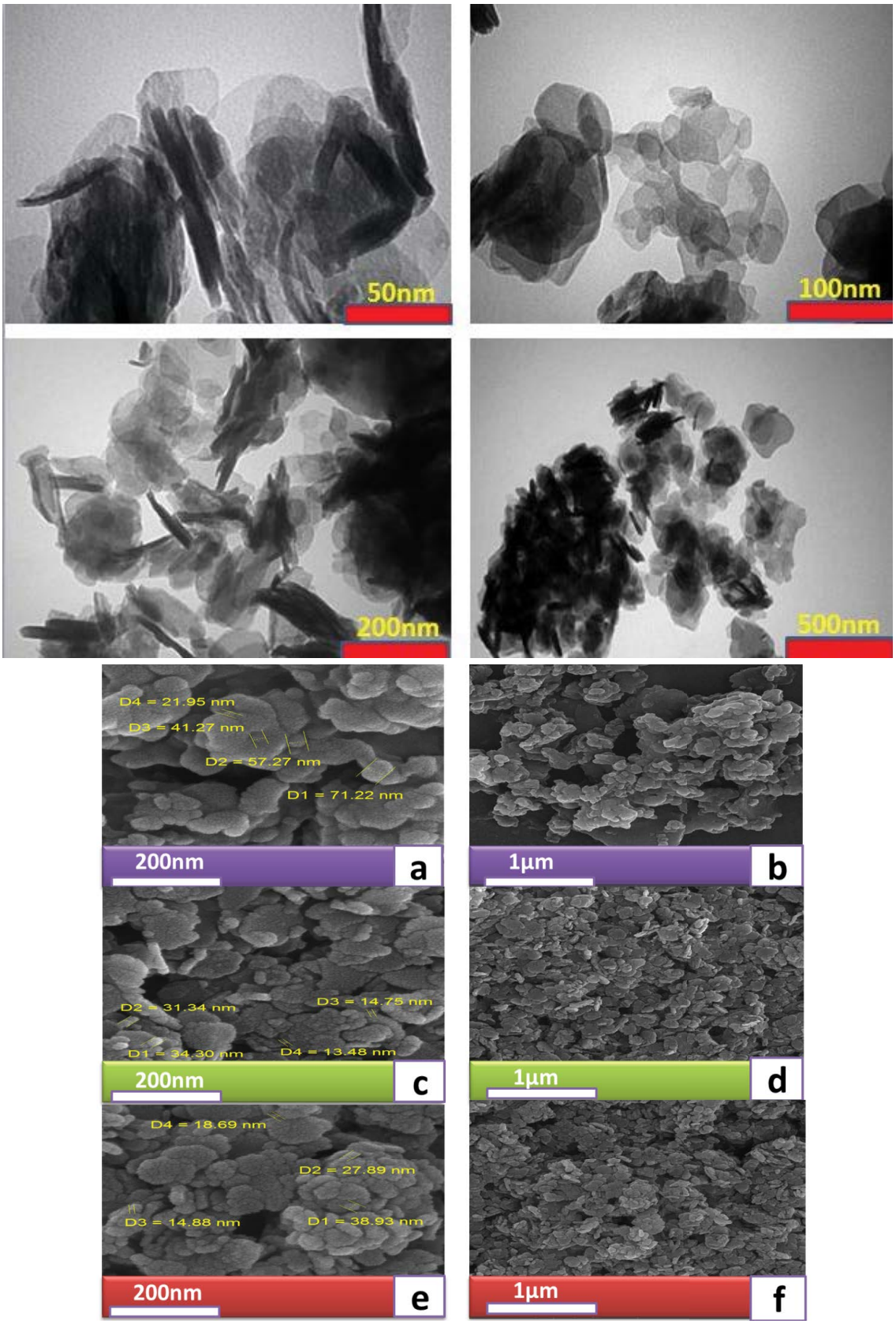

Fig. 1. (A) TEM images of Zn-Co-Al-LDH@CN and (B) SEM images of CN (a and b), Zn-Co-Al-LDH (c and d) and Zn-Co-LDH@CN (e and f).

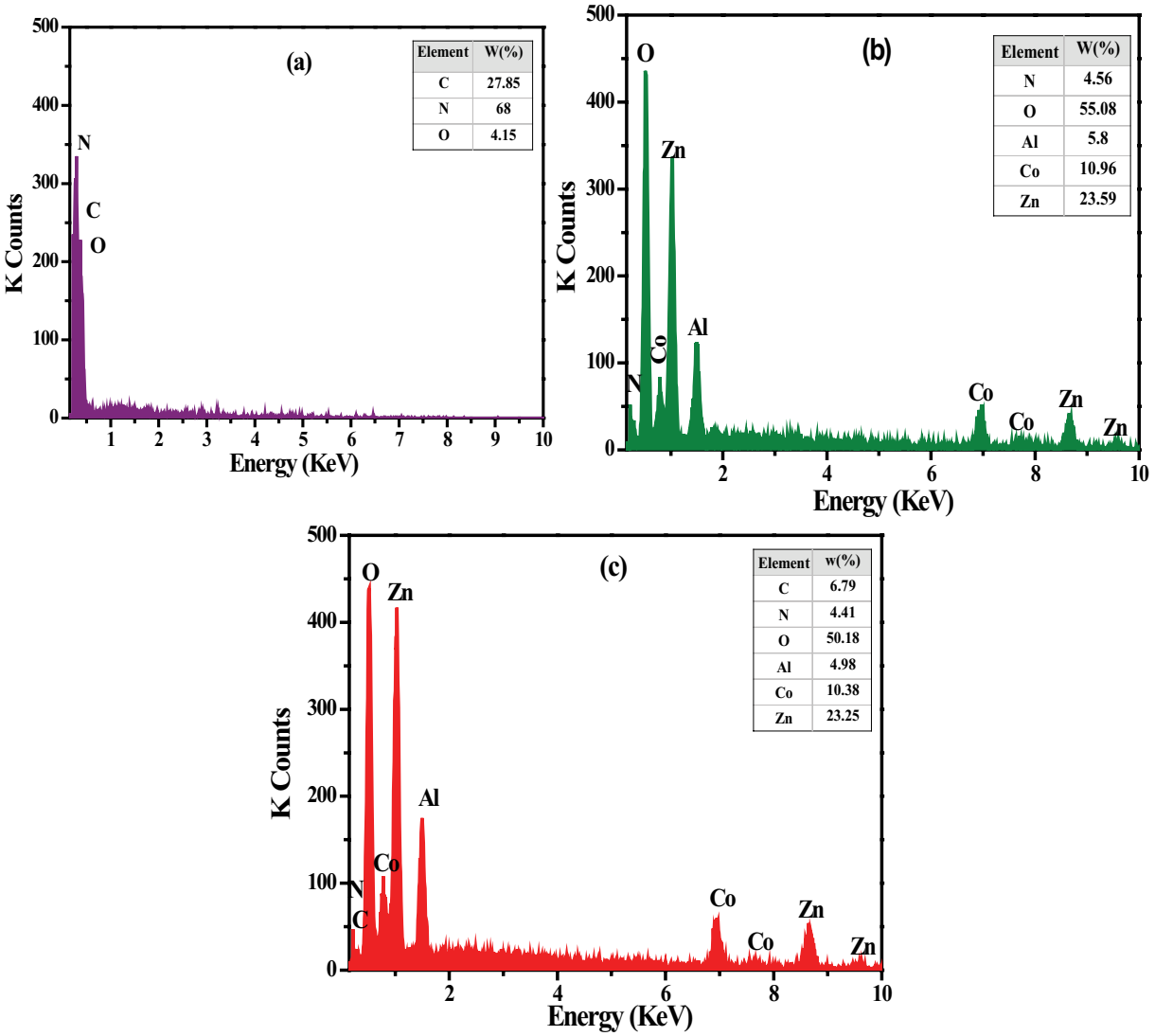

Fig. 2. EDX micrographs of CN (a), Zn-Co-Al-LDH (b) and Zn-Co-Al-LDH@CN (c).

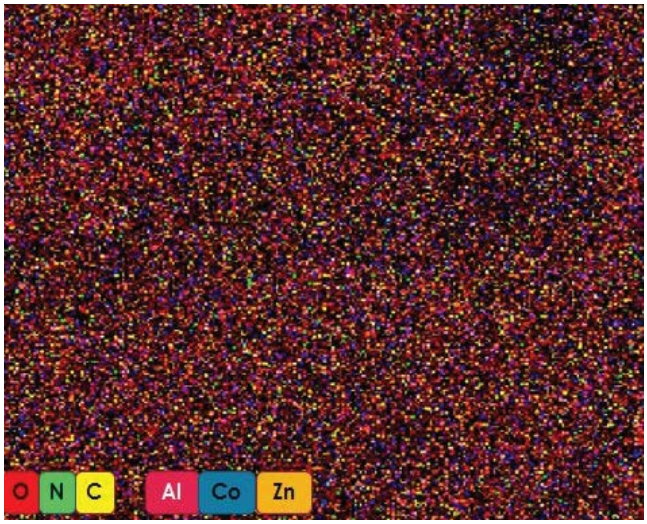

Fig. 3. EDX dot mapping micrographs of Zn-Co-Al-LDH@CN.

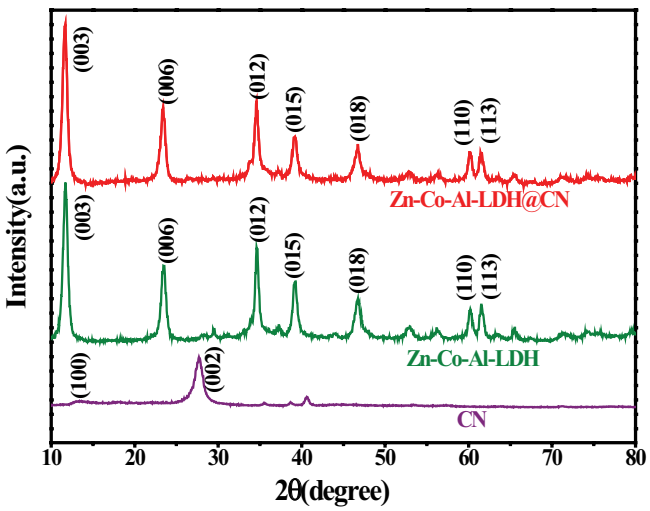

Fig. 4. XRD patterns of pristine CN, Zn-Co-Al-LDH and Zn-Co-Al-LDH@CN samples.

was not adjusted by the surface area of the heterojunctions. The synergy among the components of Zn-Al-Co-LDH@CN heterojunctions was primarily due to the exceptional degradation performance [29].

3.1.4. FT-IR Results

The FT-IR analysis was conducted to recognize the surface functional groups of synthesized samples (Fig. 6). The high degradation potential of CR by the photocatalyst is due to the existence of several functional groups on its surface [23]. Peaks observed in pure and synthesized photocatalyst at 1,651 and 3,452 cm^{-1} are due to H–O–H and O–H vibrations. The band observed at 1,060 cm^{-1} is ascribed to C–O stretching vibration [30], while the peak at 1,126 cm^{-1} is attributed to C–N vibration [31]. The band within the range of 500–1,000 cm^{-1} is attributed to CO–OH, Al–OH and Zn–OH stretching vibrations [32]. A series of peaks observed between 1,200 to 1,650 cm^{-1} is a result of regular stretching modes of CN heterocycles [21].

3.1.5. Diffuse reflectance spectroscopy results

Light-responsive features of fabricated samples were analyzed by UV-Visible diffuse reflectance spectra (DRS). UV-Vis spectra of CN in Fig. 7a show an absorption edge at 460 nm implying its visible-light absorption features. In UV-Vis spectra of Zn-Al-Co-LDH, two particular absorption bands are observed at wavelengths within the ranges of 200–300 nm and 500–600 nm attributed to ligand-to-metal charge transfer in the nanocomposite layer [33–35]. This common light absorption of Zn-Al-Co-LDH in the visible range can also be observed in the Zn-Al-Co-LDH@CN heterojunction demonstrating the strong coordination between CN and Zn-Al-Co-LDH [29].

To calculate the bandgap of photocatalysts, an extrapolation was done based on the linear part of $(\alpha h\nu)^2$ vs. $(h\nu)$ plot, using the following equation:

$$(\alpha h\nu)^2 = K\left(h\nu - E_g\right) \quad (1)$$

where α is the absorption coefficient, K is the absorption index and $h\nu$ is the photon energy (eV). The value of E_g indicates the bandgap energy of the photocatalyst [24].

According to Fig. 7b obtained by using Eq. (1), the bandgap of CN, Zn-Al-Co-LDH and Zn-Al-Co-LDH@CN nanocomposites is 2.7, 4.2, and 2.8 eV, respectively. This demonstrates the major role of CN in decreasing the bandgap energy of the photocatalyst and enhancing the photocatalytic degradation of CR. CN, with such characteristics as high conductivity and stable photosensitivity, leads to decreasing recombination of electron holes produced during photocatalysis which improves the catalytic oxidation of CR [29].

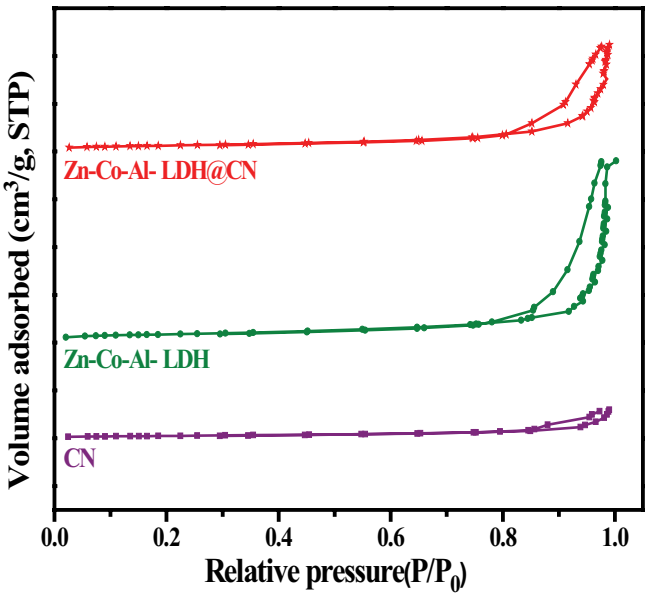

Fig. 5. Nitrogen adsorption/desorption isotherms of CN, Zn-Co-Al-LDH and Zn-Co-Al LDH@CN samples.

Table 1
Surfaces area and porosity parameters of Zn-Co-Al-LDH, CN and Zn-Co-Al-LDH@CN samples

Samples	S_{BET} ($m^2\ g^{-1}$)	V_{Total} ($cm^3\ g^{-1}$)	D_p (nm)
Zn-Co-Al-LDH	61.655	0.573	37.177
CN	17.441	0.091921	21.082
Zn-Co-Al-LDH@CN	44.945	0.3436	30.58

3.2. Contribution of various processes to CR degradation

The UV-Vis spectra of CR degraded by Zn-Al-Co-LDH@CN are presented in Fig. 8. Two main adsorption bands in the visible region of 330 and 497 nm wavelengths, ascribed

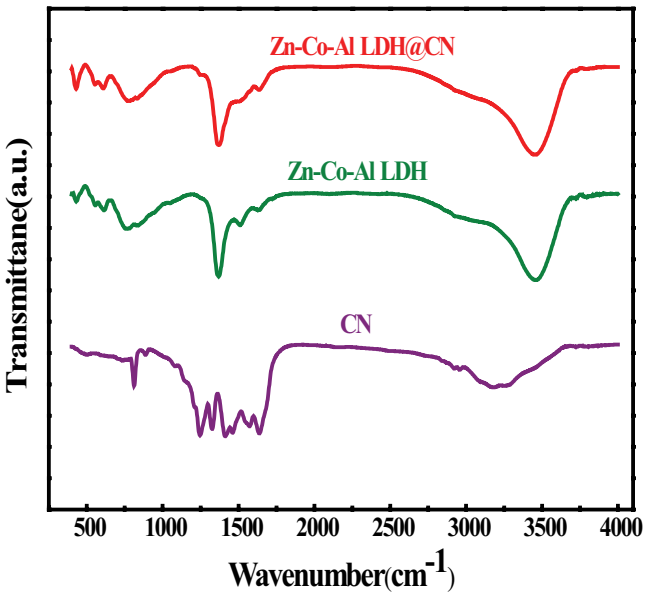

Fig. 6. FT-IR spectra of pristine CN, Zn-Co-Al-LDH and Zn-Co-Al-LDH@CN samples.

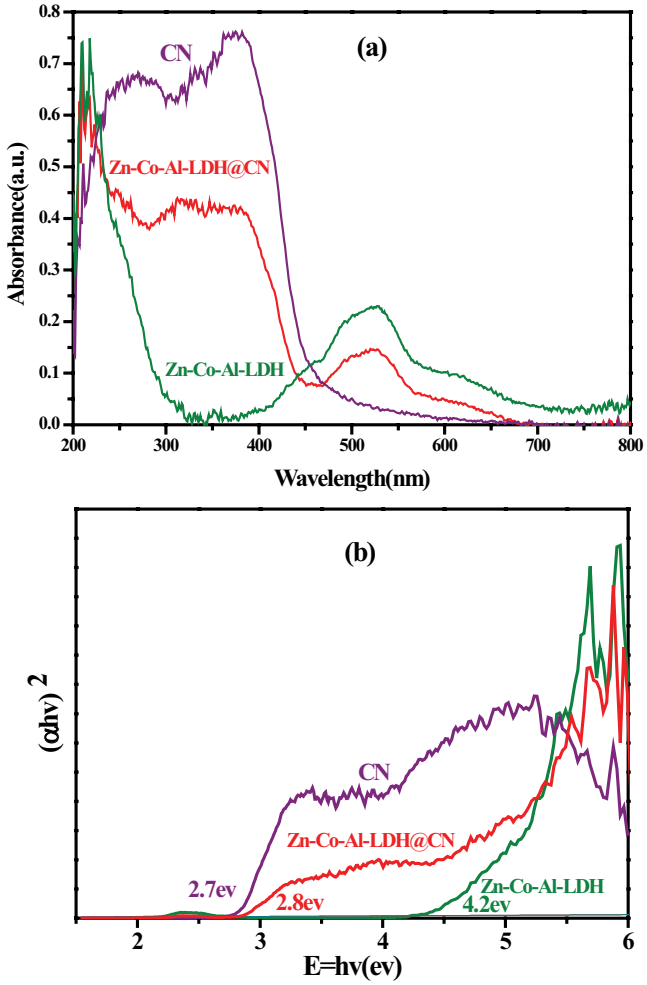

Fig. 7. (a) UV-Vis DRS patterns of CN, Zn-Co-Al-LDH and Zn-Co-Al-LDH@CN samples and (b) bandgap of the CN, Zn-Co-Al-LDH and Zn-Co-Al-LDH@CN samples.

to the adsorption of the CR chromophore group, were used to characterize the UV-Vis spectra of CR. Most adsorption peaks were diminished instantly and almost all peaks vanished completely within 180 min.

Degradation of CR takes place in two parts. Firstly, dyes are adsorbed to the catalysts by anion exchange and secondly, organic dyes are degraded under the visible light irradiation through the photocatalysis process. To comprehend the role of adsorption in the photocatalytic process, the degradation efficiency (DE) of CR by adsorption in dark and photocatalysis under light is presented in Fig. 8. The DE percentage of CR was determined by the following equation [36]:

$$\mathrm{DE}\% = \frac{\left(C_0 - C_t\right)}{C_0} \times 100 \tag{2}$$

where C_0 (mg L^{-1}) is the initial concentration of the organic dye and C_t (mg L^{-1}) is the concentration of CR at the reaction time.

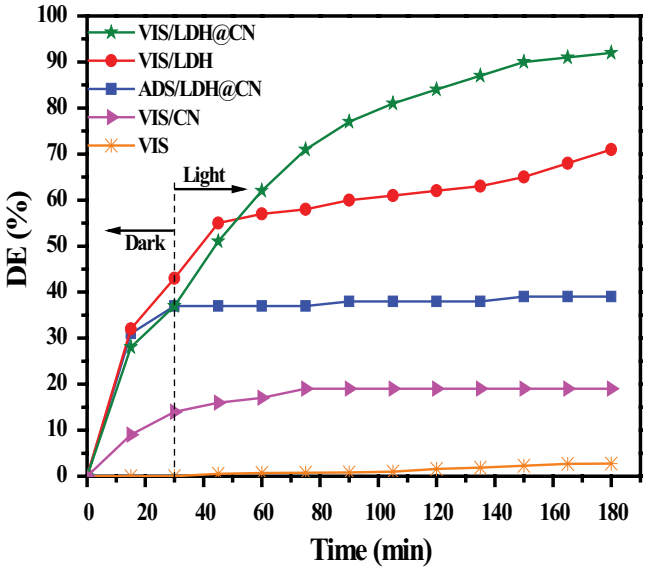

Fig. 8. Comparison of the degradation efficiency of CR using various processes. Experimental conditions: [photocatalyst dosage] = 0.15 g L^{-1}; [initial CR concentration] = 40 mg L^{-1}; pH 6; contact time = 180 min; temperature: 25°C (Vis: visible, ADS: adsorption).

The photocatalytic performance of CN, Zn-Al-Co-LDH, and Zn-Al-Co-LDH@CN for CR degradation was evaluated in an aqueous solution under visible-light irradiation and the same experimental conditions. The control experiment without the catalyst showed that CR was extremely steady under visible-light irradiation with only 2.75% of degradation during 180 min. Furthermore, the control experiment conducted in dark proved that pollutant elimination was exclusively triggered by either light illumination or catalyst. It signifies that the synergy among the components of Zn-Al-Co-LDH@CN heterojunctions was largely liable for the remarkable degradation in performance [29]. Subject to the presence of CN particles, the CR removal rate was 19%. Once the Zn-Al-Co-LDH was used as a photocatalyst, the DE of CR increased considerably to 70.40%. The LDHs have proved to be the perfect photocatalysts for decomposing dye contaminants. Photocatalytic properties of LDHs are related to their surface electrical features due to the presence of various interlayer anions [29]. In addition, LDHs decrease the electron–hole recombination proportion due to the existence of surface cavities as trapping sites to capture electrons with transitional metals [29].

The redox features of cobalt (Co) were efficiently used for degrading various organic contaminants [37]. Similar to other Co-based compounds such as Co_3O_4, $CoSe_2$ and Co–Pi, cobalt hydroxide acted as a low-cost cocatalyst for improving the photocatalytic performance of various semiconductors. In fact, cobalt, zinc, and aluminum hydroxide contributed to improving the photocatalytic performance of Zn-Al-Co-LDH. The separation of photogenerated charge carriers can be proficiently improved by cobalt hydroxide and consequently, can repress their recombination [38]. Incorporation of CN into Zn-Al-Co-LDH lattice generated an efficient photocatalyst with 92.7% CR

removal efficiency under ultraviolet-visible light according to the following equations [39]:

$$\text{Zn-Co-Al-LDH@CN} + h\nu \rightarrow \text{Zn-Co-Al-LDH@CN}\left(h^+ + e^-\right) \quad (3)$$

$$\text{Zn-Co-AL-LDH@CN}\left(e_{CB}^-\right) + O_2 \rightarrow \text{Zn-Co-AL-LDH@CN} + O_2^{\bullet -} \quad (4)$$

$$\text{Zn-Co-Al-LDH@CN}\left(h_{VB}^+\right) + H_2O \rightarrow \text{Zn-Co-Al-LDH@CN} + H^+ + {}^{\bullet}OH \quad (5)$$

where h_{VB}^+ is hole conduction in a valence band, e_{CB}^- is the electron conduction band and hν is the photon energy (eV). Once the CN particles were incorporated into the Zn-Al-Co-LDH lattice, the aggregated Zn-Al-Co-LDH nanostructures were consistently scattered on the nanocomposite surface. Therefore, this generates free oxidizing radicals as a result of exposure to more active reaction sites [24]. In addition, CN with an extended and delocalized π-conjugated system could offer a particular conductivity. This conductivity facilitates transmission of electrons to Zn-Al-Co-LDH and consequently, decreases the recombination of electron-hole pairs which oxidizes organic pollutants in the solution [40]. OH^- groups were converted into active OH radicals by the photogenerated holes. In addition, a portion of oxygen that was transformed to superoxide radicals during the electron transport process could be combined with H^+ to form hydroxyl radicals. Hydroxyl and superoxide radicals could oxidize macromolecules of dye to small molecules more suitable for adsorption [41].

3.3. Kinetic studies

As exhibited in Fig. 9, results of kinetic studies were fitted to the pseudo-first-order kinetic model with Eq. (6):

$$\ln\left(\frac{C_0}{C_t}\right) = K_{app}t \quad (6)$$

where K_{app} is the rate constant (min^{-1}). According to Fig. 9, the optimum value for K_{app} is identified by applying Zn-Al-Co-LDH@CN as the photocatalyst in CR degradation under UV-Vis light. The K_{app} values of bare CN and Zn-Al-Co-LDH under UV-Vis light were 3×10^{-4} and 33×10^{-4} min^{-1}, respectively, while the integration of CN with Zn-Al-Co-LDH under UV-Vis light irradiation resulted in a K_{app} value of 140×10^{-4} min^{-1}. The process conducted under UV-Vis light with Zn-Al-Co-LDH@CN photocatalyst had a K_{app} value of approximately four times that of K_{app} value with Zn-Al-Co-LDH photocatalyst. It showed the important role of CN in the enhancement of CR degradation.

The synergy percent was calculated using Eq. (7) to assess the role of CN in Zn-Al-Co-LDH@CN nanocomposite in CR degradation as follows:

$$\text{Synergy}(\%) = \frac{K_{app}\text{UV/Zn-Co-Al-LDH@CN} - \left(K_{app}\text{UV/CN} + K_{app}\text{UV/Zn-Co-Al-LDH}\right)}{K_{app}\text{UV/Zn-Co-Al-LDH@CN}} \quad (7)$$

Using the obtained K_{app} values, the synergy percent was 74% with the integration of CN particles into Zn-Al-Co-LDH structure [24].

3.4. Effect of operational conditions on CR degradation

3.4.1. Dosage

To achieve the optimum operating conditions during the photodegradation of CR subject to the presence of Zn-Al-Co-LDH@CN nanocomposite, the impact of Zn-Al-Co-LDH@CN dosage was evaluated in this set of experiments. According to Fig. 10, the degradation efficiency of CR was influenced by the Zn-Al-Co-LDH@CN dosage. It is evident that by increasing the dosage of catalyst from 0.1 to 0.25 g L^{-1}, CR removal efficiency was enhanced from 66% to 97%. In principle, the removal efficiency in the photocatalysis process is enhanced at the higher amounts of photocatalyst due to the production of higher amounts of h^+, $O^{2\bullet}$ and $^{\bullet}OH$. However, determining the optimum value of photocatalyst dosage is important from an economical aspect. With an increase in catalyst dosage from 0.15 to 0.25 g L^{-1}, no considerable improvement was observed in the CR degradation efficiency and the adsorption capacity; thus, 0.15 g L^{-1} was selected as the optimum dosage.

3.4.2. Concentration

As illustrated in Fig. 11, CR degradation efficiency (DE) reduced by increasing the initial CR concentration. By increasing the initial CR concentration from 30 to

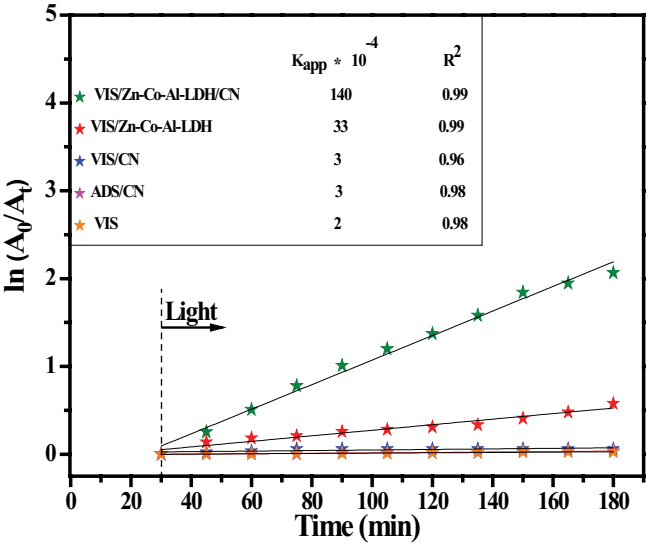

Fig. 9. Kinetic analysis results based on pseudo-first-order model. Experimental conditions: [photocatalyst dosage] = 0.15 g L^{-1}; [initial CR concentration] = 40 mg L^{-1}; pH 6; temperature: 25°C (Vis: visible, ADS: adsorption).

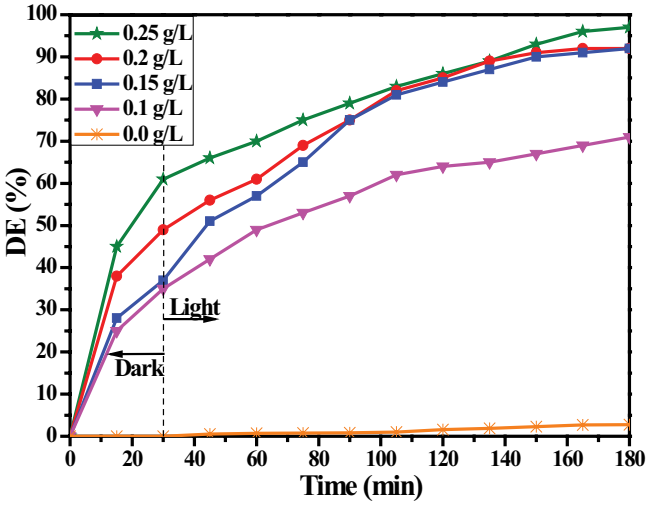

Fig. 10. Effect of photocatalyst dosage on photocatalytic degradation of CR. Experimental conditions: [initial CR concentration] = 40 ppm; pH 6; contact time = 180 min; temperature: 25°C.

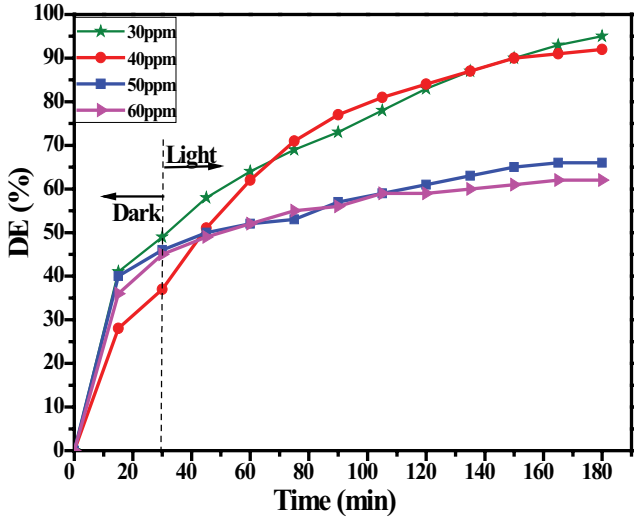

Fig. 11. Effect of CR concentration on its photocatalytic degradation by Zn-Co-Al-LDH@CN. Experimental conditions: [photocatalyst dosage] = 0.15 g L^{-1}; pH 6; contact time = 180 min; temperature: 25°C.

60 ppm, DE was reduced from 95% to 62%. As the concentration of CR in the photoreactor increases, higher amounts of h^+, $O^{2\bullet}$ and $^\bullet OH$ are required to reach a convincing photocatalytic DE [42].

3.4.3. pH

Initial pH affects both the surface charge of the catalyst and solution features; therefore, it has a significant role in heterogeneous catalytic treatment systems [23]. In this regard, the photocatalytic performance of Zn-Al-Co-LDH@CN heterojunction in aqueous solution was evaluated in several initial pH values of 4.7, 6.0, 7.7, and 9.7 (Fig. 12). For pH values lower than 3, the chemical structure of CR

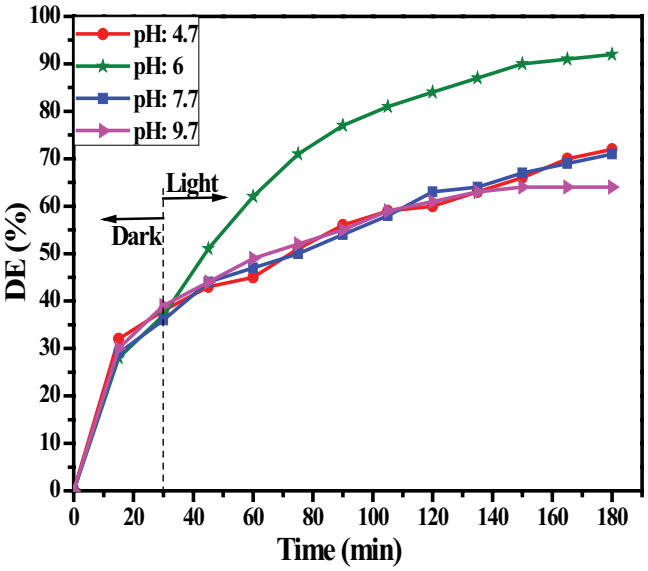

Fig. 12. Effect of initial pH on photocatalytic degradation of CR. Experimental conditions: [initial CR concentration] = 40 ppm; [photocatalyst dosage] = 0.15 g L^{-1}; contact time = 180 min; temperature: 25°C.

was changed; therefore, the pH value was selected from pH 4 [1]. The natural initial pH of CR aqueous solution with 40 ppm concentration was 6.12. Decreasing the pH value in an aqueous solution from 6.5 to 4.5 led to a significant decrease in the degradation efficiency. Meanwhile, there was a considerable decline in the degradation performance in an alkaline pH region (pH 7.5 and 9.5). Regarding maximum DE, pH 6 was selected as the optimum value for the test of experiment. Therefore, adjusting the pH was no longer necessary. Doing the treatment process at the natural pH of the solution is considered a priority [43].

3.5. Free radical enhancers

Persulfate and hydrogen peroxide were added to the photoreactor to enhance the catalytic conversion of the target dye contaminant. According to experiments, the Zn-Al-Co-LDH@CN dosage was selected 0.15 g L^{-1}. The CR degradation was intensified by adding both persulfate ions source and hydrogen peroxide (Fig. 13). The augmentation effects of hydrogen peroxide and persulfate ions on DE are due to the production of OH and $SO_4^{\bullet-}$ presented in Eqs. (8) and (9) [44]:

In the presence of H_2O_2:

$$H_2O_2 + e^- \rightarrow OH^- + {}^\bullet OH \quad (8)$$

In the presence of persulfate ions:

$$S_2O_8^{2-} + h\nu \rightarrow 2SO_4^{\bullet-} \quad (9)$$

Subject to the presence of persulfate ions with 3 mM concentration, approximately 97% conversion of CR after the elapsed time of 90 min was observed, caused by producing sulfate radicals with a high oxidizing potential [45].

However, a lower removal rate of 95% was detected by adding hydrogen peroxide. This may be attributed to the radical scavenging properties of hydrogen peroxide molecules as shown in Eqs. (10) and (11) [42,46]:

$$H_2O_2 + {}^{\bullet}OH \rightarrow H_2O + HO_2^{\bullet} \quad (10)$$

$$HO_2^{\bullet} + {}^{\bullet}OH \rightarrow H_2O + O_2 \quad (11)$$

Addition of oxidants increased the degradation percentage at a lower contact time (Fig. 13).

3.6. Free radical scavengers

The presence of organic and inorganic free radical scavenging compounds in aquatic media is unavoidable in real conditions. Therefore, it is necessary to understand the impact of these scavenging compounds on the photocatalytic degradation of CR and specify the function of various free oxidizing radicals in the degradation of the target contaminant. As illustrated in Fig. 14, the presence of benzoquinone (BQ), EDTA and ethanol (ETOH) negatively affected the photocatalytic performance of the nanocomposite. Ethanol, BQ and EDTA were recognized as $^{\bullet}OH$, superoxide radical anions ($O^{2\bullet-}$), and hole (h^+) scavengers, respectively [29]. Among them, EDAT had the greatest inhibiting effect on the photocatalytic degradation efficiency of CR through direct removal of $^{\bullet}OH$ from the bulk solution. In general, the inhibiting effect of radical species on decomposing CR was in the following order: $h^+ > O^{2\bullet} > {}^{\bullet}OH$. The Zn-Al-Co-LDH components trap photo-generated electrons and increase the number of h^+_{VB} for continuous degradation of CR [47]. Ao et al. [48] also reported that photocatalytic degradation of the target pollutant decreased further via the presence of EDTA as a hole scavenger compared to BQ as a notable $O^{2\bullet}$ scavenger.

Regarding inorganic scavengers, all anions had a certain degree of inhibiting effect on the degradation of the target contaminant. In contrast to sodium sulfate (Na_2SO_4) and sodium carbonate (Na_2CO_3), NaCl had the highest radical scavenging impact during the photocatalytic decomposition of CR (Fig. 15):

For chloride ions [46]:

$$Cl^- + {}^{\bullet}OH \rightarrow Cl^{\bullet} + OH^- \quad (12)$$

$$Cl^{\bullet} + Cl^- \rightarrow Cl_2^{\bullet-} \quad (13)$$

For carbonate ions [49]:

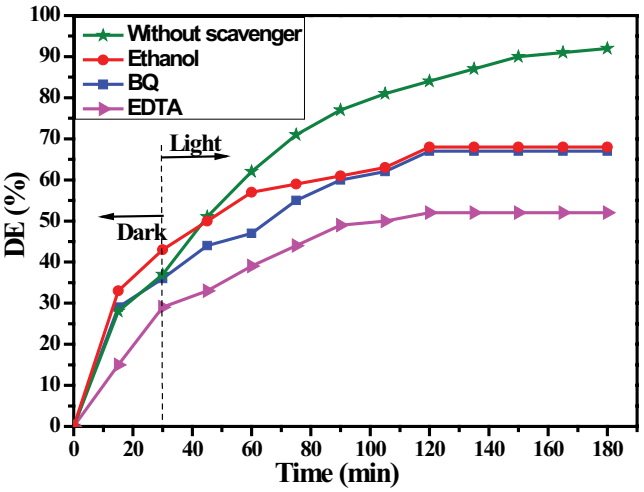

Fig. 14. Effect of organic scavengers on the decomposition of CR. Experimental conditions: [photocatalyst dosage] = 0.15 g L^{-1}; [initial CR concentration] = 40 ppm; pH 6; contact time = 180 min; [scavenger dosage] = 3 mM; temperature: 25°C.

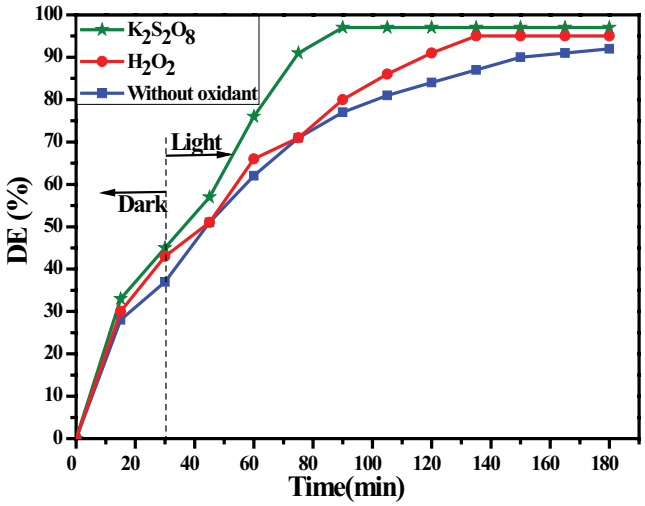

Fig. 13. Effect of oxidants (H_2O_2 and $K_2S_2O_8$) on photocatalytic degradation of CR. Experimental conditions: [photocatalyst dosage] = 0.15 g L^{-1}; [initial CR concentration] = 40 ppm; pH 6; contact time = 180 min; [oxidant dosage] = 3 mM; temperature: 25°C.

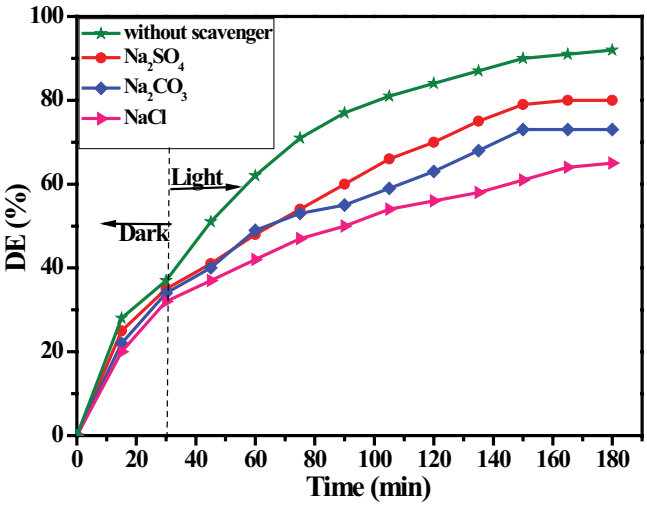

Fig. 15. Effect of inorganic scavengers on the decomposition of CR. [Photocatalyst dosage] = 0.15 g L^{-1}; [initial CR concentration] = 40 ppm; pH 6; contact time = 180 min; [scavenger dosage] = 3 mM; temperature: 25°C.

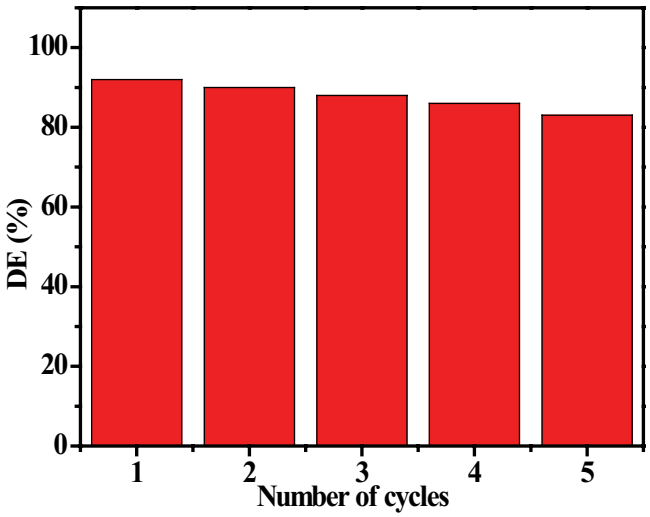

Fig. 16. Variations of degradation efficiency within five consecutive photocatalytic runs. Experimental conditions: [initial CR concentration] = 40 ppm; [photocatalyst dosage] = 0.15 g L^{-1}; contact time = 180 min; temperature: 25°C.

$$CO_3^{2-} + OH \rightarrow CO_3^{\bullet -} + H_2O \quad (14)$$

For sulfate ions [24]:

$$SO_4^{2-} + {}^{\bullet}OH \rightarrow SO_4^{\bullet -} + OH^- \quad (15)$$

3.7. Reusability potential of nanocomposite

To assess the applicability of the catalyst in the full-scale operation, the reusability of Zn-Al-Co-LDH@CN photocatalyst was studied. The regeneration studies for evaluating the degradation efficiency of the nanocomposite were conducted in five successive cycles. According to Fig. 16, less than a 10% drop in the removal efficiency of CR occurred at the end of the fifth run, demonstrating the desirable reusability of the synthesized photocatalyst within successive runs of operation. In conclusion, the present Zn-Al-Co-LDH@CN heterojunctions can be regarded as a promising material for practical applications in environmental protection due to its excellent degradation activity and high photostability [29].

3.8. Mineralization

The COD analysis was carried out to specify the extent of the mineralization of CR during the degradation process. During the degradation process, CO_2, H_2O and other by-products can be formed [24]. Although decolorization of CR was somewhat faster than the degree of mineralization, approximately 71% of COD and 52% of total organic carbon (TOC) removal was yielded during UV-Vis light in 400 min ([photocatalyst dosage] = 0.15 g L^{-1}, [initial CR concentration] = 40 mg L^{-1} and pH 6). During dye oxidation, small organic molecular fragments such as acetic acids, epoxides, aldehydes, ketones, etc. were produced leading to a COD residual. The COD produced from these small new-formed molecules can be further reduced by a biological process [27]. The drop in TOC values suggests that CO_2 molecules are formed simultaneously with other volatile organic compounds such as formaldehyde and acetaldehyde during the oxidation process [28].

4. Conclusion

Zn-Al-Co-LDH@CN nanocomposite synthesized by co-precipitation method has an exceptional photocatalytic activity for CR oxidation. Zn-Al-Co-LDH@CN nanocomposite was used as an efficient photocatalyst for the decontamination of CR dye-polluted solutions under UV-V is light in a wide range of pH conditions. The maximum degradation efficiency was achieved under the neutral pH of 6. CN particles were appropriately incorporated into the structure of Zn-Al-Co-LDH and effectively improved the photocatalytic efficiency in CR degradation. Under the same operational conditions, Zn-Al-Co-LDH@CN nanocomposite demonstrated a greater photocatalytic activity, with a 92.7% removal percentage in comparison with Zn-Al-Co-LDH, with 70.4% removal rate and pure CN with a 19% removal percentage. This justifies the scattering of LDH nanostructures on CN surface and separation of charge carriers by utilizing cobalt hydroxide. In fact, the fast recombination proportion of photocatalytic generated holes and electrons was impeded by the existence of both LDH and CN particles. Pseudo-first-order kinetic model perfectly fitted to the experimental data. The formation of free oxidizing radicals and degradation of CR molecules were significantly increased by adding persulfate ions. The existence of EDTA decreased the effectiveness of the photocatalysis process, confirming the negative effect of free oxidizing radicals, particularly hole (h^+), on the degradation and conversion of CR. An insignificant decline in the photocatalytic activity of the Zn-Al-Co-LDH@CN nanocomposite during five consecutive runs was observed. In conclusion, the synthesized nanocomposite is a reasonable alternative for decontaminating dye-contained aqueous solutions under UV-Vis light.

References

[1] M. Kafil, S.B. Nasab, H. Moazed, J. Jokiniemi, A. Lähde, A. Bhatnagar, Efficient removal of azo dyes from water with chitosan/carbon nanofloas a novel nanocomposite synthesized by pyrolysis technique, Desal. Water Treat., 142 (2018) 308–320.
[2] C.R. Holkar, A.J. Jadhav, D.V. Pinjari, N.M. Mahamuni, A.B. Pandit, A critical review on textile wastewater treatments: possible approaches, J. Environ. Manage., 182 (2016) 351–366.
[3] V.S. Munagapati, D.S. Kim, Adsorption of anionic azo dye Congo red from aqueous solution by Cationic Modified Orange Peel Powder, J. Mol. Liq., 220 (2016) 540–548.
[4] P. Petronela, C. Cojocaru, N. Olaru, P.Samoila, A. Airinei, M. Ignat, L. Sacarescu, D. Timpu, Novel rare earth (RE-La, Er, Sm) metal doped ZnO photocatalysts for degradation of Congo-Red dye: synthesis, characterization and kinetic studies, J. Environ. Manage., 239 (2019) 225–234.
[5] P. Wang, D.H.L. Ng, M. Zhou, J. Li, Freely standing MgAl-layered double hydroxides nanosheets and their derived metal oxides on g-C_3N_4 thin-layer designed for obtaining synergic effect of adsorption and photocatalysis, Appl. Clay Sci., 178 (2019) 105–131.
[6] K. Sathishkumar, M.S. AlSalhi, E. Sanganyado, S. Devanesan, A. Arulprakash, A. Rajasekar, Sequential electrochemical oxidation and bio-treatment of the azo dye Congo red and

textile effluent, J. Photochem. Photobiol., B, 200 (2019) 111655, doi: 10.1016/j.jphotobiol.2019.111655.
[7] L. Aljerf, High-efficiency extraction of bromocresol purple dye and heavy metals as chromium from industrial effluent by adsorption onto a modified surface of zeolite: kinetics and equilibrium study, J. Environ. Manage., 225 (2018) 120–132.
[8] S. Ye, M. Yan, X. Tan, J. Liang,G. Zeng, H. Wu, H. Wang, Facile assembled biochar-based nanocomposite with improved graphitization for efficient photocatalytic activity driven by visible light, Appl. Catal., B, 250 (2019) 78–88.
[9] S. Ye, G. Zeng, X. Tan, H. Wu, J. Liang, B. Song, X. Li, Nitrogen-doped biochar fiber with graphitization from *Boehmeria nivea* for promoted peroxymonosulfate activation and non-radical degradation pathways with enhancing electron transfer, Appl. Catal., B, 269 (2020) 118850, doi: 10.1016/j.apcatb.2020.118850.
[10] M. Qi, L. Fan, Y. Shen, H. Zou, X. Tian, D. Liu, S. Li, Improved visible-light-induced photocatalytic performance of ZnAl layered double hydroxide by incorporation of Ni^{2+}, J. Nanosci. Nanotechnol., 18 (2018) 753–760.
[11] P. Gholami, A. Khataee, R.D. Soltani, L. Dinpazhoh, A. Bhatnagar, Photocatalytic degradation of gemifloxacin antibiotic using Zn-Co-LDH@biochar nanocomposite, J. Hazard. Mater., 382 (2020) 121070, doi: 10.1016/j.jhazmat.2019.121070.
[12] M. Daud, M.S. Kamal, F. Shehzad, M.A.A. Harthi, Graphene/layered double hydroxides nanocomposites: a review of recent progress in synthesis and applications, Carbon, 104 (2016) 241–252.
[13] K. Parida, L. Mohapatra, N. Baliarsingh, Effect of Co^{2+} substitution in the framework of carbonate intercalated Cu/Cr LDH on structural, electronic, optical, and photocatalytic properties, J. Phys. Chem. C, 116 (2012) 22417–22424.
[14] K. Parida, M. Satpathy, L. Mohapatra, Incorporation of Fe^{3+} into Mg/Al layered double hydroxide framework: effects on textural properties and photocatalytic activity for H_2 generation, J. Mater. Chem., 22 (2016) 7350–7357.
[15] Y. Fu, F. Ning, S. Xu, H. An, M. Shao, M. Wei, Terbium doped ZnCr-layered double hydroxides with largely enhanced visible light photocatalytic performance, J. Mater. Chem. A, 4 (2016) 3907–3913.
[16] N. Baliarsingh, L. Mohapatra, K. Parida, Design and development of a visible light harvesting Ni-Zn/Cr-CO_3^{2-} LDH system for hydrogen evolution, J. Mater. Chem. A, 1 (2013) 4236–4243.
[17] M.S. Quezada, G.R. Ortiz, V. Suárez, G.M. Mendoza, L.L. Rojas, E.N. Cerón, F. Tzompantzi, S. Robles, R. Gómez, A. Mantilla, Photodegradation of phenol using reconstructed Ce doped Zn/Al layered double hydroxides as photocatalysts, Catal. Today, 271 (2016) 213–219.
[18] D. Jiang, T. Wang, Q. Xu, D. Li, S. Meng, M. Chen, Perovskite oxide ultrathin nanosheets/g-C_3N_4 2D-2D heterojunction photocatalysts with significantly enhanced photocatalytic activity towards the photodegradation of tetracycline, Appl. Catal., B, 201 (2017) 617–628.
[19] J. Liu, J. Li, X. Bing, D.H. Ng, X. Cui, F. Ji, D.D. Kionga, ZnCr-LDH/N-doped graphitic carbon-incorporated g-C_3N_4 2D/2D nanosheet heterojunction with enhanced charge transfer for photocatalysis, Mater. Res. Bull., 102 (2018) 379–390.
[20] S. Tonda, S. Kumar, M. Bhardwaj, P. Yadav, S. Ogale, g-C_3N_4/NiAl-LDH 2D/2D hybrid heterojunction for high-performance photocatalytic reduction of CO_2 into renewable fuels, ACS Appl. Mater. Interfaces, 10 (2018) 2667–2678.
[21] W.J. Ong, L.L. Tan, Y.H. Ng, S.T. Yong, S.P. Chai, Graphitic carbon nitride (g-C_3N_4)-based photocatalysts for artificial photosynthesis and environmental remediation: are we a step closer to achieving sustainability?, Chem. Rev., 116 (2016) 7159–7329.
[22] W.K. Jo, S. Kumar, S. Eslava, S. Tonda, Construction of Bi_2WO_6/RGO/g-C_3N_4 2D/2D/2D hybrid Z-scheme heterojunctions with large interfacial contact area for efficient charge separation and high-performance photoreduction of CO_2 and H_2O into solar fuels, Appl. Catal., B, 239 (2018) 586–598.
[23] H. Lu, M. Sui, B. Yuan, J. Wang, Y. Lv, Efficient degradation of nitrobenzene by Cu-Co-Fe-LDH catalyzed peroxymonosulfate to produce hydroxyl radicals, Chem. Eng. J., 357 (2018) 140–149.
[24] M. Ghasemi, A. Khataee, P. Gholami, R.D.C. Soltani, Template-free microspheres decorated with Cu-Fe-NLDH for catalytic removal of gentamicin in heterogeneous electro-Fenton process, J. Environ. Manage., 248 (2019) 109236, doi: 10.1016/j.jenvman.2019.07.007.
[25] Y. Wu, H. Wang, Y. Sun, T. Xiao, W. Tu, X. Yuan, G. Zeng, S. Li, J.W. Chew, Photogenerated charge transfer via interfacial internal electric field for significantly improved photocatalysis in direct Z-scheme oxygen-doped carbon nitrogen/CoAl-layered double hydroxide heterojunction, Appl. Catal., B, 227 (2018) 530–540.
[26] S. Tonda, S. Kumar, S. Kandula, V. Shanker, Fe-doped and -mediated graphitic carbon nitride nanosheets for enhanced photocatalytic performance under natural sunlight, J. Mater. Chem. A, 2 (2014) 6772–6780.
[27] Y. Wang, L. Dou, H. Zhang, Nanosheet array-like palladium-catalysts Pd_x/rGO@CoAl-LDH via lattice atomic-confined in situ reduction for highly efficient heck coupling reaction, ACS Appl. Mater. Interfaces, 9 (2017) 38784–38795.
[28] S. Jorfi, R.D.C. Soltani, M. Ahmadi, A. Khataee, M. Safari, Sono-assisted adsorption of a textile dye on milk vetch-derived charcoal supported by silica nanopowder, J. Environ. Manage., 187 (2016) 111–121.
[29] W.K. Jo, S. Tonda, Novel CoAl-LDH/g-C_3N_4/RGO ternary heterojunction with notable 2D/2D/2D configuration for highly efficient visible-light-induced photocatalytic elimination of dye and antibiotic pollutants, J. Hazard. Mater., 368 (2019) 778–787.
[30] G. Jie, M.A. Lowe, H.D. Abruna, Spongelike nanosized Mn_3O_4 as a high-capacity anode material for rechargeable lithium batteries, Chem. Mater., 23 (2011) 3223–3227.
[31] L.H. Su, X.G. Zhang, Effect of carbon entrapped in Co-Al double oxides on structural restacking and electrochemical performances, J. Power Sources, 172 (2007) 999–1006.
[32] S. Erdemoğlu, S.K. Aksu, F. Sayılkan, B. Izgi, M. Asiltürk, H. Sayılkan, F. Frimmel, Ş. Güçer, Photocatalytic degradation of Congo red by hydrothermally synthesized nanocrystalline TiO_2 and identification of degradation products by LC-MS, J. Hazard. Mater., 155 (2008) 469–476.
[33] S. Kumar, M.A. Isaacs, R. Trofimovaite, L. Durndell, C.M. Parlett, R.E. Douthwaite, B. Coulson, M.C. Cockett, K. Wilson, A.F. Lee, P25@CoAl layered double hydroxide heterojunction nanocomposites for CO_2 photocatalytic reduction, Appl. Catal., B, 209 (2017) 394–404.
[34] K. Wang, L. Zhang, Y. Su, D. Shao, S. Zeng, W. Wang, Photoreduction of carbon dioxide of atmospheric concentration to methane with water over CoAl-layered double hydroxide nanosheets, J. Mater. Chem. A, 6 (2018) 8366–8373.
[35] C. Rudolf, B. Dragoi, A. Ungureanu, A. Chirieac, S. Royer, A. Nastro, E. Dumitriu, NiAl and CoAl materials derived from takovite-like LDHs and related structures as efficient chemoselective hydrogenation catalysts, Catal. Sci. Technol., 4 (2014) 179–189.
[36] H.Y. Xu, L.C. Wu, H. Zhao, L.G. Jin, S.Y. Qi, Synergic effect between adsorption and photocatalysis of metal-free g-C_3N_4 derived from different precursors, PLoS One, 10 (2015) 0142616, doi: 10.1371/journal.pone.0142616.
[37] A. Jawad, Y. Li, X. Lu, Z. Chen, W. Liu, G. Yin, Controlled leaching with prolonged activity for Co-LDH supported catalyst during treatment of organic dyes using bicarbonate activation of hydrogen peroxide, J. Hazard. Mater., 289 (2015) 165–173.
[38] L.J. Zhang, R. Zheng, S. Li, B.K. Liu, D.J. Wang, L.L. Wang, T.F. Xie, Enhanced photocatalytic H_2 generation on cadmium sulfide nanorods with cobalt hydroxide as cocatalyst and insights into their photogenerated charge transfer properties, ACS Appl. Mater. Interfaces, 6 (2014) 13406–13412.
[39] R.D.C. Soltani, A.R. Khataee, M. Mashayekhi, Photocatalytic degradation of a textile dye in aqueous phase over ZnO nanoparticles embedded in biosilica nanobiostructure, Desal. Water Treat., 57 (2016) 13494–13504.

[40] S. Patnaik, S. Martha, G. Madras, K. Parida, The effect of sulfate pre-treatment to improve the deposition of Au-nanoparticles in a gold-modified sulfated g-C_3N_4 plasmonic photocatalyst towards visible light induced water reduction reaction, Phys. Chem. Chem. Phys., 18 (2016) 28502–28514.
[41] M. Lan, G. Fan, L. Yang, F. Li, Significantly enhanced visible-light-induced photocatalytic performance of hybrid zn-cr layered double hydroxide/graphene nanocomposite and the mechanism study, Ind. Eng. Chem. Res., 53 (2014) 12943–12952.
[42] S. Sajjadi, A. Khataee, R.D. Soltani, N. Bagheri, A. Karimi, A.E. Azar, Implementation of magnetic Fe_3O_4@ZIF-8 nanocomposite to activate sodium percarbonate for highly effective degradation of organic compound in aqueous solution, J. Ind. Eng. Chem., 68 (2018) 406–415.
[43] A. Khataee, S. Sajjadi, A. Hasanzadeh, B. Vahid, S.W. Joo, One-step preparation of nanostructured martite catalyst and graphite electrode by glow discharge plasma for heterogeneous electro-Fenton like process, J. Environ. Manage., 199 (2017) 31–45.
[44] F. Sepyani, R.D. Soltani, S. Jorfi, H. Godini, M. Safari, Implementation of continuously electro-generated Fe_3O_4 nanoparticles for activation of persulfate to decompose amoxicillin antibiotic in aquatic media: UV_{254} and ultrasound intensification, J. Environ. Manage., 224 (2018) 315–326.
[45] L.W. Matzek, K.E. Carter, Activated persulfate for organic chemical degradation: a review, Chemosphere, 15 (2016) 178–188.
[46] O. Acisli, A. Khataee, R.D. Soltani, S. Karaca, Ultrasound-assisted Fenton process using siderite nanoparticles prepared via planetary ball milling for removal of reactive yellow 81 in aqueous phase, Ultrason. Sonochem., 35 (2017) 210–218.
[47] R. Lu, X. Xu, J. Chang, Y. Zhu, S. Xu, F. Zhang, Improvement of photocatalytic activity of TiO_2 nanoparticles on selectively reconstructed layered double hydroxide, Appl. Catal., B, 111 (2012) 389–396.
[48] Y. Ao, D. Wang, P. Wang, C. Wang, J. Hou, J. Qian, Enhanced photocatalytic properties of the 3D flower-like Mg-Al layered double hydroxides decorated with Ag_2CO_3 under visible light illumination, Mater. Res. Bull., 80 (2016) 23–29.
[49] M. Karaca, M. Kiranşan, S. Karaca, A. Khataee, A. Karimi, Sonocatalytic removal of naproxen by synthesized zinc oxide nanoparticles on montmorillonite, Ultrason. Sonochem., 31 (2016) 250–256.